



Wavepacket Modeling and Full-scale Military Jet Noise Beamforming Analyses

Blaine M. Harker,¹ Kent L. Gee,² Tracianne B. Neilsen³
Brigham Young University, Provo, UT, 84602

Alan T. Wall⁴
Air Force Research Laboratory, Wright-Patterson Air Force Base, OH, 45433

and

Michael M. James⁵
Blue Ridge Research and Consulting, LLC, Asheville, NC, 28801

Because jet noise consists of extended, partially correlated sources, a multi-wavepacket model is appropriate to simulate jet noise field levels as well as the appropriate spatial coherence properties within the field. Here, the Hybrid method is used to reconstruct the levels and coherence properties of the source region for multi-wavepacket numerical models. The beamforming source results are then propagated to the acoustic field, where they show good agreement with benchmark levels and coherence lengths. The Hybrid method is further applied to a planar measurement of noise near a high-performance military aircraft, and the beamforming results are propagated to a ground-based microphone array. Sound levels and coherence lengths generated by the beamforming results show good agreement with benchmark measurements over a range of frequencies that contribute significantly to the overall radiation. Results indicate that the multi-wavepacket representation is an improvement over single-wavepacket models, which do not incorporate spatiotemporal features of the radiation.

Nomenclature

| | |
|---------------------------|---|
| \mathbf{C} | = cross-spectral matrix |
| f | = frequency |
| \mathbf{G} | = Green function response matrix |
| $G(\vec{x}_m, \vec{x}_s)$ | = Green function response to \vec{x}_m from \vec{x}_s |
| k | = acoustic wavenumber |
| \mathbf{L}^{-1} | = beamforming regularization matrix |
| \mathbf{P}_f | = partial field matrix |
| \mathbf{p} | = vector of pressure measurements |
| $\hat{p}(\vec{x}_m)$ | = pressure measurement at \vec{x}_m |
| \mathbf{Q} | = beamforming response matrix |
| \mathbf{q} | = vector of source strengths |
| $q(\vec{x}_s)$ | = source strength at \vec{x}_s |
| \mathbf{W} | = matrix of columnated steering vectors |
| \vec{x}_m | = array measurement location |
| \vec{x}_s | = source location |

¹ Graduate Student, Dept. of Physics and Astronomy, N283 ESC, AIAA Student Member.

² Associate Professor, Dept. of Physics and Astronomy, N283 ESC, AIAA Senior Member.

³ Part-Time Assistant Professor, Dept. of Physics and Astronomy, N283 ESC, AIAA Member.

⁴ Postdoctoral Research Fellow, Battlespace Acoustics Branch, AFRL 711 HPW/RHCB, AIAA Member.

⁵ Senior Principal Engineer, 29 N Market St, Suite 700, AIAA Member.

α = spatial wavenumber
 ν^2 = penalization parameter
 λ = wavelength

I. Introduction

WAVEPACKET models continue to be an important asset in working towards a better understanding of jet noise. Different types of wavepackets exist, including those obtained from visualization methods, which have been shown to accurately represent the turbulence features present in jet flows,¹ as well as equivalent-source wavepacket models that describe the acoustic radiation from the turbulent mixing noise.^{2,3} While not necessarily a unique modeling tool, wavepacket distributions have provided an efficient means of representing the level-based features of acoustic radiation beyond the hydrodynamic field of the jet. Suzuki and Colonius⁴ developed a method to detect instability waves using an eigenfunction approach, similar to beamforming. Du and Morris⁵ applied conventional beamforming to simulated far-field jet noise data to obtain the acoustic complex pressure at the jet lipline, which was then decomposed using a wavepacket shape. Papamoschou developed a cost-function approach to simulate a jet noise field based on a seven-parameter wavepacket representation.² However, these models have not attempted to match the spatiotemporal field characteristics. A single wavepacket, while able to simulate the radiation levels of jet mixing noise in the dominant radiation direction, is unable to reproduce the spatially varying coherence properties of the field due to its self-coherent nature. However, a superposition of self-coherent, mutually-incoherent wavepackets can be used to estimate these temporal characteristics in the field. This paper shows advanced beamforming algorithms can be used with such a multi-wavepacket model for jet noise.

Inverse methods, particularly beamforming, have previously been applied to field measurements of jet noise in order to reconstruct equivalent acoustic sources. However, while traditional beamforming methods have been used to localize some aeroacoustic sources, they have suffered in attempts to localize the extended, partially-correlated noise found in jet noise sources.⁶ Recent developments have allowed for improved beamforming source localization methods. Some methods have also recently been developed that provide the correlation properties which exist between these sources.⁷ A derivative of a deconvolution beamforming approach (DAMAS⁸) called DAMAS-C incorporates the potential correlation which may exist between sources.⁶ CLEAN-SC has also been developed for this purpose,⁹ although studies have shown difficulties using this method in the presence of extended, correlated sources.¹⁰ Dougherty¹⁰ introduced the generalized inverse technique as a way to localize extended, coherent sources. This method utilizes a geometrically-defined smoothing operator and Tikhonov regularization to produce a unique solution. It also produces a source cross-spectral matrix that can be used to predict the radiated field. Padois *et al.*¹¹ introduced a similar technique, the Hybrid method, which also incorporates a regularization method. However, instead of a smoothing operator, they introduce a beamforming regularization matrix that improves the regularization procedure and can successfully localize extended correlated sources. Both methods have shown success in localizing extended, coherent source distributions, although neither has yet to be applied to full-scale tactical aircraft noise measurements.

The focus of the present study is two-fold. First, we demonstrate the importance of a jet noise wavepacket distribution that matches both the measured levels of the acoustic radiation and the coherence properties of the measured field. Second, it is shown that through the use of the Hybrid method, a cross-spectral matrix describing an equivalent acoustic source can be constructed that predicts both the levels and the coherence properties of the field. These properties are validated on numerical and experimental datasets using benchmark cases.

In this paper, the cross-beamforming method and Hybrid method are reviewed, as well as the particular modifications required for use with the measurement geometry in the present study. In addition, the wavepacket methodology is described for a single wavepacket, as well as a system of wavepackets that can reproduce the levels and coherence properties of the acoustic field. The beamforming methods are illustrated using single wavepacket numerical simulation, and an example is shown where the Hybrid method successfully reproduces the levels and coherence properties of an acoustic field resulting from a source distribution of multiple wavepackets. Finally, the Hybrid method is applied to a planar measurement of complex pressures taken in the geometric near field of an F-22A Raptor. It is shown that the beamforming results, when propagated into the field, predict the levels and coherence properties of other benchmark measurements.

II. Methods

Beamforming methods have been developed which are appropriate for application to spatially extended sources with arbitrary correlation. Two methods, cross beamforming and the Hybrid Method (i.e., hybrid beamforming), are

described here. These methods are important for the development of more complete equivalent source models of jet noise. Numerical examples are provided to illustrate the performance of these beamforming methods.

The numerical validation is accomplished using a coherent source distribution known as a wavepacket. While a single wavepacket is self-coherent and, therefore, generates a completely coherent field, the inclusion of multiple self-coherent but mutually incoherent wavepackets can be used to generate an acoustic field that resembles the levels and coherence lengths typical of those measured in the vicinity of a jet flow. It will be shown that while both cross beamforming and the Hybrid Method reconstruct the distribution and coherence properties of the source, the Hybrid Method is more capable of capturing the properties of the source that, when used to predict the levels and coherence properties of the field, show better agreement when compared to field benchmark measurements.

(A) Beamforming Methods

Unlike traditional far-field beamforming methods where the distance from source to array is much larger than the array size, beamforming in the geometric near field of a source distribution requires additional considerations and leads to improved resolution. Here, we describe the cross-beamforming method,⁶ which can be used when sources are not mutually incoherent. In addition, we summarize the Hybrid Method developed by Padois *et al.*¹¹ Both methods will be applied in Section II(C) to numerical simulations to determine their capabilities and limitations. The hybrid method will be applied to experimental measurements of full-scale jet noise in Section III.

1. Cross beamforming

Cross beamforming is an extension of traditional beamforming that is capable of identifying source coherence characteristics. An array consisting of M microphones is used to measure the pressure field, $\hat{p}(\vec{x}_m)$, at each array element location, \vec{x}_m , and for a given frequency, f (which is not explicitly referenced for convenience). If we assume that S sources, each with a complex source strength of $q(\vec{x}_s)$, are located at positions \vec{x}_s , we can describe the acoustic pressure in matrix form as

$$\hat{p}(\vec{x}_m) = G(\vec{x}_m, \vec{x}_s)q(\vec{x}_s). \quad (1)$$

Here, the free-field Green function, $G(\vec{x}_m, \vec{x}_s)$, incorporates the propagation from the source to the measurement location. Equation (1) can conveniently be rewritten in matrix format, such that

$$\mathbf{p} = \mathbf{G} \mathbf{q}, \quad (2)$$

where the vector of acoustic pressures, \mathbf{p} , is $[M, 1]$ in length, the vector of complex source strengths, \mathbf{q} , is $[S, 1]$, and the Green function matrix \mathbf{G} , is $[M, S]$ in size and accounts for the free-field propagation from each source to each array element. We seek to solve for \mathbf{q} , which is accomplished by solving a similar inverse problem:

$$\mathbf{q} = \mathbf{W}^\dagger \mathbf{p}, \quad (3)$$

where \dagger is the conjugate transpose operator. The operator, \mathbf{W}^\dagger , is the steering vector matrix and can be formulated in multiple ways. In the traditional matrix beamforming response, $\mathbf{W}^\dagger = \mathbf{G}^\dagger$;¹² this definition is also used in the present study. The problem can also be generalized such that \mathbf{G}^\dagger is the Moore-Penrose generalized inverse.¹⁰ As an alternative approach, various steering vector methods have been proposed, which enhance various aspects of source characteristics.¹³ The resulting cross-beamforming response follows as

$$\mathbf{Q}_{\text{XBF}} = \mathbf{q}\mathbf{q}^\dagger = \mathbf{W}^\dagger \mathbf{p}\mathbf{p}^\dagger \mathbf{W} = \mathbf{W}^\dagger \mathbf{C} \mathbf{W}, \quad (4)$$

where the quantity $\mathbf{C} \equiv \mathbf{p}\mathbf{p}^\dagger$ is the cross-spectral matrix corresponding to the acoustic measurements. \mathbf{Q}_{XBF} is a cross-spectral matrix of the source reconstruction estimated by the cross beamforming, and diagonal elements of \mathbf{Q}_{XBF} contain the individual source powers commonly reported in conventional beamforming. The off-diagonal elements of \mathbf{Q}_{XBF} are referred to as the cross-beamforming elements, which represent the simultaneous steering of the array pressures to two locations along the source region. The magnitude of the estimated cross-beamforming response, $Q_{\text{XBF}}(\vec{x}_{s_1}, \vec{x}_{s_2})$, relative to the corresponding individual source responses [$Q_{\text{XBF}}(\vec{x}_{s_1}, \vec{x}_{s_1})$ and $Q_{\text{XBF}}(\vec{x}_{s_2}, \vec{x}_{s_2})$], is significant if there exists a degree of coherence between corresponding source locations, \vec{x}_{s_1} and \vec{x}_{s_2} . Techniques, such as DAMAS-C, rely on the cross-beamforming response to model sources that exhibit some degree of mutual coherence.⁶

Once the cross-beamforming response, \mathbf{Q}_{XBF} , is obtained, the validity of the source reconstruction can be evaluated by comparing the predicted field to additional measurements. \mathbf{Q}_{XBF} is propagated by defining a new Green function, \mathbf{G}_p , that includes steering vectors for the additional locations.¹⁰ The cross-spectral matrix of field pressures, \mathbf{C}_p , at those locations can be modeled using

$$\mathbf{C}_p = |\mathbf{G}_p \mathbf{q}|^2 = \mathbf{G}_p \mathbf{Q}_{\text{XBF}} \mathbf{G}_p^\dagger, \quad (5)$$

and compared to measurements.

2. The Hybrid Method

In most cases, the inverse problem associated with obtaining beamforming results is underdetermined because of the non-uniqueness of the potential source distribution. Regularization methods can be used to introduce constraints (e.g., which attenuate measurement noise) to produce a unique solution.^{10, 11} A common approach used in holography methods to improve conditioning of the problem is called Tikhonov regularization,¹¹ in which a regularization parameter is added to the generalized inverse of the Green function. The solution to Equation (2) then becomes

$$\mathbf{q} = (\mathbf{G}^\dagger \mathbf{G} + \nu^2 \mathbf{L}^\dagger \mathbf{L})^{-1} \mathbf{G}^\dagger \mathbf{p}, \quad (6)$$

where ν^2 is a penalization parameter, and \mathbf{L} is a square weighting matrix. In classical Tikhonov regularization, \mathbf{L} is set to be the identity matrix and ν^2 is set such that uncertainty in the measurement and low-level noise are not amplified through the process of inverting \mathbf{G} . Methods to determine ν^2 include the Morozov discrepancy procedure and the generalized cross validation procedure. These are discussed in Ref. [14].

The Hybrid Method adds additional information to the standard Tikhonov regularization by defining a beamforming regularization matrix,

$$\mathbf{L}^{-1} = \left[\text{Diag} \left(\frac{\sqrt{\text{diag}(\mathbf{Q}_{\text{XBF}})}}{\sqrt{\|\text{diag}(\mathbf{Q}_{\text{XBF}})\|_\infty}} \right) \right], \quad (7)$$

where \mathbf{L}^{-1} consists of a square matrix with elements formed from the individual source powers from $\text{diag}(\mathbf{Q}_{\text{XBF}})$. Here, $\text{diag}(\cdot)$ takes the diagonal elements of a matrix and $\text{Diag}(\cdot)$ forms a diagonal matrix of these elements, $\|\cdot\|_\infty$ is the infinity norm, and $\sqrt{\cdot}$ is applied element-wise. The beamforming regularization matrix inputs additional information about the beamforming problem to the regularization process. Incorporating Equation (7) into Equation (6) and simplifying produces:

$$\mathbf{q}' = \mathbf{L}^{-1} (\mathbf{G}^\dagger \mathbf{G} + \nu^2 \mathbf{I})^{-1} \mathbf{G}^\dagger \mathbf{p}, \quad (8)$$

where $\underline{\mathbf{G}} = \mathbf{G} \mathbf{L}^{-1}$, and \mathbf{q}' is the estimated vector of source powers. Using Equation (8), the Hybrid Method is developed such that

$$\mathbf{Q}_{\text{HBF}} = \mathbf{q}' \mathbf{q}'^\dagger = \mathbf{L}^{-1} (\mathbf{J} \underline{\mathbf{G}}^\dagger) \mathbf{C} (\underline{\mathbf{G}} \mathbf{J}^\dagger) (\mathbf{L}^{-1})^\dagger, \quad (9)$$

where

$$\mathbf{J} = (\underline{\mathbf{G}}^\dagger \underline{\mathbf{G}} + \nu^2 \mathbf{I})^{-1}. \quad (10)$$

Similar to the cross-beamforming method, the hybrid-beamforming response, \mathbf{Q}_{HBF} , is a matrix with auto- and cross-beamforming elements. In addition, it can be used as an equivalent source and propagated to the field at any desired location.

3. Additional beamforming considerations

In Section III, the Hybrid method is applied to an experimental dataset that was obtained in the geometric near-field of an F-22A Raptor. The requirements of the experiment necessitate additional considerations in the beamforming methods, including the use of nonsimultaneous measurements, which necessitates the decomposition of the measurement into partial fields using singular value decomposition. Also, adaptations must be made for beamforming to both a direct and image source to account for the half-space environment of the measurement. These are now discussed in turn

Beamforming using partial fields. The entire measurement plane is measured in a patch-and-scan method, with each of the 30 measurement locations of the 90-element planar array contributing a ‘‘patch’’ of the overall measurement plane. While this planar array is moved about various positions along the measurement plane, a fixed reference array records synchronously. The non-synchronous measurements are then phase-aligned on a frequency-by-frequency basis in a process called partial field decomposition (PFD). A singular value decomposition is performed on measurement array and reference array data. Each of the resultant partial fields (i.e., eigenvectors) is then phase-aligned using the reference array, resulting in a linearly independent set of self-coherent, mutually incoherent partial

fields, each of which span the measurement plane, and that together sum to reproduce the total measurement plane. Details of the PFD method are described in Ref [15]. The process of applying partial fields to beamforming methods is accomplished by either operating on each partial field measurement, \vec{p}_f , separately ($\mathbf{C} = \vec{p}_f \cdot \vec{p}_f^\dagger$) or by creating a matrix, \mathbf{P}_f , with columns consisting of the partial fields, and operating on all partial fields together ($\mathbf{C} = \mathbf{P}_f \cdot \mathbf{P}_f^\dagger$). Additional beamforming steps proceed as normal.

Beamforming to Image Sources. When operating in a half-space environment, reflections interfere constructively and destructively with the direct sound. The beamforming method is most effective when all potential sources contributing to a measurement array are considered so as to efficiently minimize the beamforming cost function. Hence, when considering potential source distributions locations for use in beamforming, similar image source locations mirrored about the reflection plane are also simultaneously considered. These adequately account for the frequency-dependent spatial interference patterns that may be present at either the measurement or the benchmark locations.

(B) Wavepacket Modeling

Wavepackets have been used in the study of jet noise to simulate the large-scale, correlated source features in the plume.¹ A wavepacket is defined as intermittent, advecting disturbances that are correlated over distances exceeding the integral scales of turbulence.¹ In the domain of acoustic radiation, the wavepacket ansatz has also been used as a means of representing the Mach wave radiation of a supersonic jet noise,² and separate wavepacket studies have modeled the turbulent mixing noise associated with large-scale turbulent structures.¹⁶ Here, we begin with an equivalent acoustic source wavepacket model and evaluate its radiation pattern, as well as the coherence properties of the predicted field (i.e., the field coherence). In particular, we show that the sound radiation from a single wavepacket cannot adequately represent the field coherence properties of a jet noise acoustic field, and that a system of multiple wavepackets is more appropriate for reproducing the jet noise levels and spatiotemporal properties. In addition, this representation can serve to validate beamforming methods that attempt to reconstruct the levels and coherence properties of an extended, partially correlated source. Both the single wavepacket and multiple-wavepacket distributions are utilized in Section II(C) for the application of cross-beamforming and the Hybrid method.

In this study, we adopt the wavepacket shape similar to the one described by Papamoschou,² who modeled the pressure fluctuations on a cylindrical surface as an axisymmetric solution to the wave equation in cylindrical coordinates and provided convenient means to control for the growth, decay and phase speed of the source. However, we make a slight adjustment to instead define source strengths along the jet centerline for a volume velocity wavepacket, as

$$Q(z) = \tanh \left[\left(\frac{z}{b_1} \right)^{g_1} \right] \left\{ 1 - \tanh \left[\left(\frac{z}{b_2} \right)^{g_2} \right] \right\} e^{i\alpha z}. \quad (11)$$

Here, α is the spatial wavenumber (valid for $\alpha \leq k$), b_1 and g_1 determine the length scale and the rate of growth of the wavepacket amplitude, and b_2 and g_2 similarly determine the length scale and rate of decay of the wavepacket. An example of a wavepacket is shown in Figure 1(a), where the properties have been defined as $b_1 = 5\lambda$, $b_2 = 3\lambda$, $g_1 = 3$, $g_2 = 1$, and $\alpha = k/2$, where k is the acoustic wavenumber. The wavepacket amplitude has been normalized, and the magnitude and real part of the wavepacket are displayed. When this single wavepacket is propagated over a large horizontal plane using Equation (5), the acoustic radiation displayed in Figure 1(c) is obtained, where x represents the horizontal distance from the jet centerline in terms of λ , and z the downstream distance from the nozzle exit plane. To provide the opportunity to evaluate the behavior of the beamforming algorithms in the presence of measurement noise, a noise floor was added such that the minimum level at all field locations is 60 dB below the maximum level present in the field. Efficient radiation of this example wavepacket occurs because $\alpha \leq k$ causing highly directional radiation with the maximum occurring at the angle ϕ (defined from the positive z axis), as

$$\phi = \cos^{-1}(\alpha/k). \quad (12)$$

In this example, $\alpha = k/2$, so $\phi = \cos^{-1}(1/2) = 60^\circ$.

For a given acoustic wavelength, λ , a single wavepacket solution has been demonstrated to successfully simulate the strong directional properties of supersonic jet noise radiation.^{2, 3, 17} However, unlike the variation which exists in field coherence of jet noise radiation, a wavepacket is self-coherent and any acoustic radiation will likewise be completely coherent. Thus, to model both the level and the coherence, a system of wavepackets, each with a different spatial wavenumber, provides a set of self-coherent but mutually incoherent sources to more accurately represent the field. An example distribution of the real part and magnitude of a multiple wavepacket source distribution is given in Figure 1(b). In this example, 30 wavepackets (chosen to ensure a smoothly-varying field) are varied only by the spatial

wavenumber, which ranges between $0.1k \leq \alpha_i \leq 0.9k$, with an average wavenumber $\langle \alpha_i \rangle = k/2$. The different wavepackets [of which five are displayed in Figure 1(b)] are weighted in amplitude such that greater weighting is given to wavepackets with a spatial wavenumber approaching $k/2$. In Figure 1(d) the corresponding acoustic radiation pattern is displayed, and a similar noise floor is added as was used in Figure 1(c). Because the average spatial wavenumber is $k/2$ and greater weighting is placed on the wavepackets with α nearest this value, the acoustic radiation resembles that of the single wavepacket. However, the directivity of the radiated lobe is slightly broader and the resultant radiation is more dispersive when compared to that of the single wavepacket radiation.

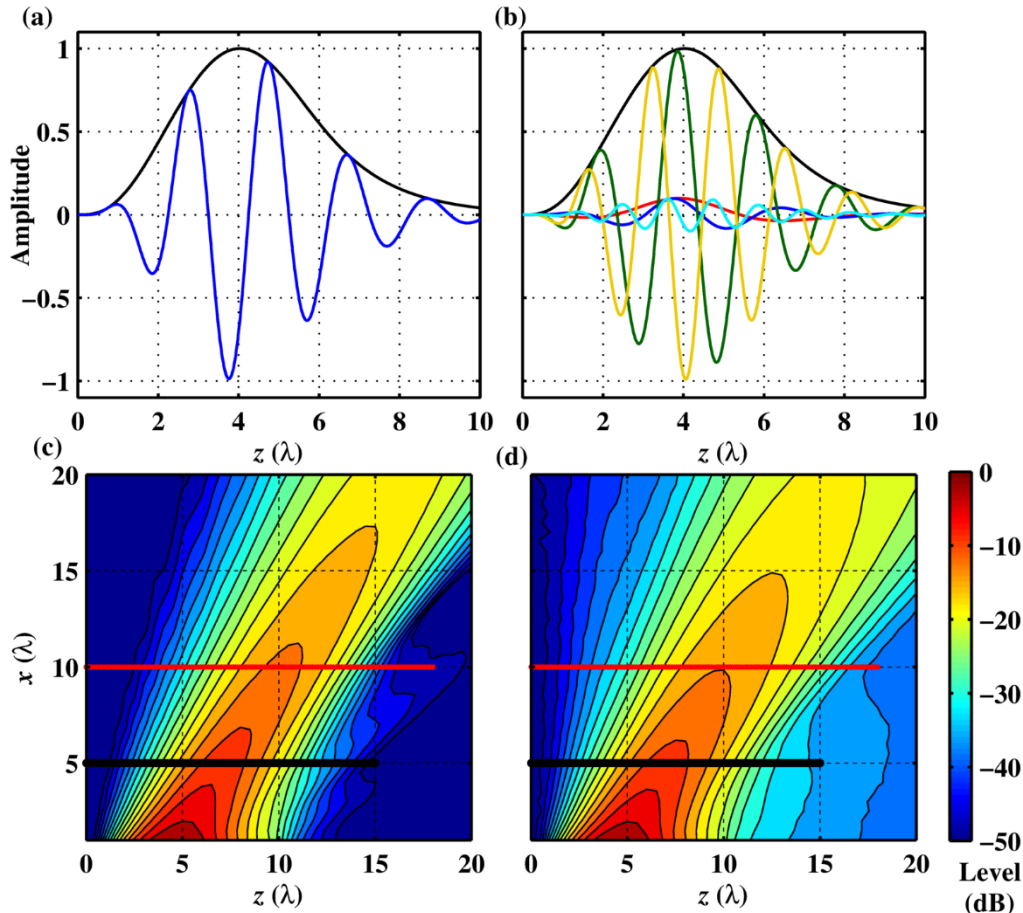


Figure 1. Wavepacket Examples. Amplitude of the magnitude and real part are shown for a) a single wavepacket source distribution and b) a source distribution consisting of multiple wavepackets with varying phase speeds. The resultant radiated fields are given for each respective source distribution are displayed in c) and d).

To investigate the coherence properties of the field, we consider a one-dimensional reference array [displayed as a red line in Figure 1(c) and (d)] that is positioned 10λ from the axial source distribution and spans 18λ . The coherence across this reference array is calculated and shown in Figure 2 for the single and multiple wavepacket sources used in Figure 1. The coherence between measurement points across the array is represented by the colorscale in Figure 2. For the field from the single wavepacket, the coherence across the array is nearly unity at all locations. The only region of low coherence is at the extreme upstream edge of the array, where radiation from wavepackets is lower in level than the simulated noise floor. The coherence across the benchmark array of the wavepacket system is shown in Figure 2(b), and, in contrast to the coherence of the single wavepacket system, shows spatially dependent coherence levels across the array. The coherence length, defined as the distance from a point to the location where coherence drops to 0.5, can be used to examine the spatiotemporal features of the radiated field. In this example, coherence lengths are highest between $5\lambda < z < 10\lambda$, although there is appreciable coherence throughout with an average coherence length of about 2λ . This illustrates that a multi-wavepacket source distribution has the potential to match complex coherence

properties of a measured sound field, such as is found in the vicinity of a high performance military aircraft, in addition to predicting the radiated sound levels.

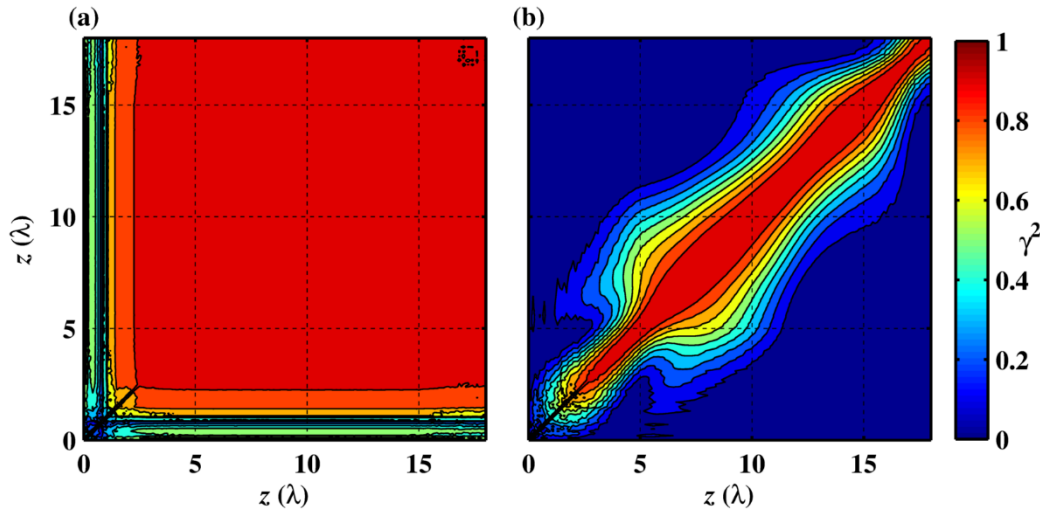


Figure 2. Field coherence of wavepacket examples. *The coherence across a reference array (displayed as a red line in Figure 1) is calculated for the field produced by a) a single wavepacket source distribution and b) a source distribution of multiple wavepackets.*

(C) Numerical Application

Two numerical validation studies are presented in which radiation from a wavepacket model is simulated along a linear array. The beamforming methods previously described are applied to this field in an attempt to reconstruct the source properties. These beamforming results are also propagated and compared with the original radiation, both with respect to level and the field coherence. In both cases, the cross-beamforming method and Hybrid method reconstruct source characteristics as well as the propagated field levels and coherence properties. In addition, the Hybrid Method is able to predict field quantities to a higher precision, especially in the presence of noise; it will be further applied in Section III to describe full-scale jet noise radiation.

The beamforming techniques begin with the field on a linear measurement array [shown as a black line in Figure 1(a)]. The linear array spans 15λ and has an interelement spacing of $\lambda/10$. Both the cross-beamforming (XBF) and hybrid-beamforming (HBF) methods are applied to measurements captured at the array. The magnitude and real part of the resulting beamforming source distribution are presented in blue in Figure 3(a) and Figure 3(b). The real part is found by multiplying the diagonal elements of \mathbf{Q} in Equation (4) by the phase arguments of the cross-spectral elements, relative to a given source reference (e.g., the maximum source location). The original source magnitude and distribution, referred to as the benchmark, are displayed in black alongside the beamforming results. In both cases, the magnitude and spatial wavenumber of the source distribution is represented by each method, with only slight discrepancies in the reconstructions. The capability to match both the magnitude and spatial wavenumber from the beamforming results affects the accuracy of propagation to the acoustic field, as described by Equation (5).

The radiated fields are shown in Figure 3(c) and Figure 3(d), which were generated using the cross-beamforming and hybrid-beamforming results, respectively. Comparing these fields to the benchmark field in Figure 1(c), we see that the general features of both predicted fields are in agreement with the benchmark acoustic field. The error between the predicted fields and the benchmark levels are shown in Figure 3(e) and Figure 3(f), which show that discrepancies are highest in regions extending beyond the spatial aperture of the measurement array (shown by the black line). In addition, the predicted field of the cross-beamforming results shows greater deviation from the benchmark levels than results from hybrid-beamforming in measurement locations where the areas of large error correspond to the noise floor. The beamforming regularization of the Hybrid Method improves the reconstruction of the source coherence properties, especially in the presence of noise, allowing for improved propagation results. Because the Hybrid Method shows improvement over the cross-beamforming method in the presence of noise, it will be solely used in the following simulations and the experimental results.

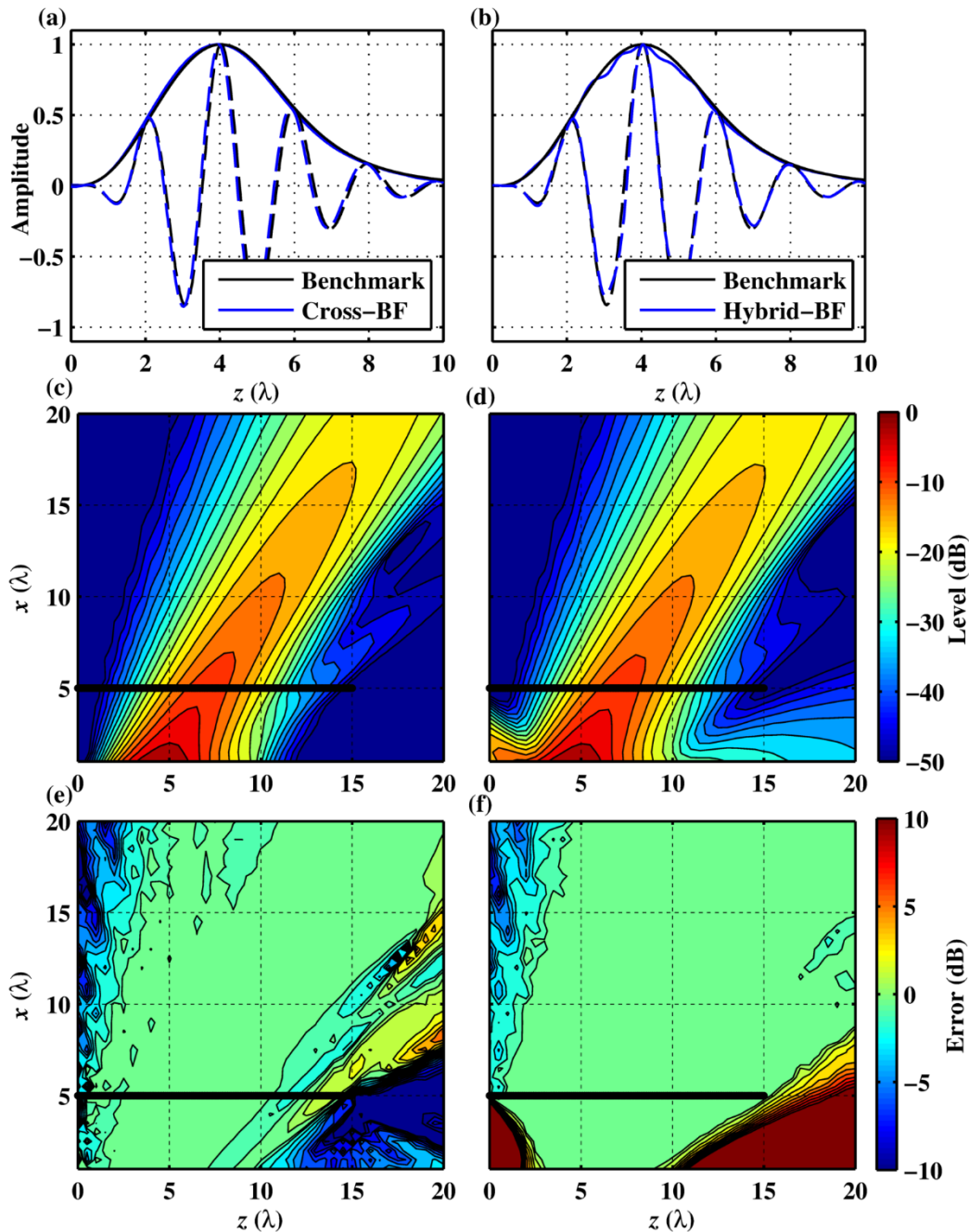


Figure 3. Single wavepacket beamforming results. Two beamforming methods are implemented on measurements taken at the array [displayed as a black line Figure 1(c)] for the single wavepacket case [Figure 1(a)]. The real part and magnitude of the source distribution benchmark are compared with (a) cross-beamforming and (b) hybrid beamforming results. (c-d) The respective beamforming results are propagated to produce a predicted field, and (e-f) the field levels errors [compare with Figure 1(c)] are shown for each method.

We now apply the hybrid-beamforming method to the multiple wavepacket source distribution presented in Figure 1(b). Measurements on the linear array with $\lambda/10$ interelement spacing, displayed as the black line in Figure 1(d), are used as input. Hybrid beamforming is applied to these measurements and the resultant beamforming source is used to create an acoustic field shown in Figure 4(a). The error of this field when compared to the field resulting from the original (benchmark) source distribution is given in Figure 4(b). The error is within 1 dB at most locations within the field, with the few exceptions occurring either in regions between the source and array or far upstream of the array

where the wavepacket sources did not significantly radiate. In the latter case, the error corresponds to the presence of measurement noise, and error between the source and measurement array can be attributed to the fact that this radiation propagates in directions not captured by the array and thus there is little information about these regions of the field.

The coherence properties of the hybrid-beamforming results on the reference array, shown by the red line in Figure 4(b), are compared to the benchmark case, shown in Figure 2(b). The predicted coherence across the reference array locations is displayed in Figure 4(c), which was calculated using the cross-spectral elements in Equation (5) (where \mathbf{Q}_{XBF} is replaced with \mathbf{Q}_{HBF}), and the corresponding error between the benchmark coherence values and the predicted coherence is given in Figure 4(d). The error of the predicted coherence is within 0.1 across nearly the entirety of the array, with the exception of the region upstream of $z = 3\lambda$. This is again due to the high noise levels relative to the radiation from the wavepacket source distribution at the location, which creates an overestimation of the coherence properties of the field.

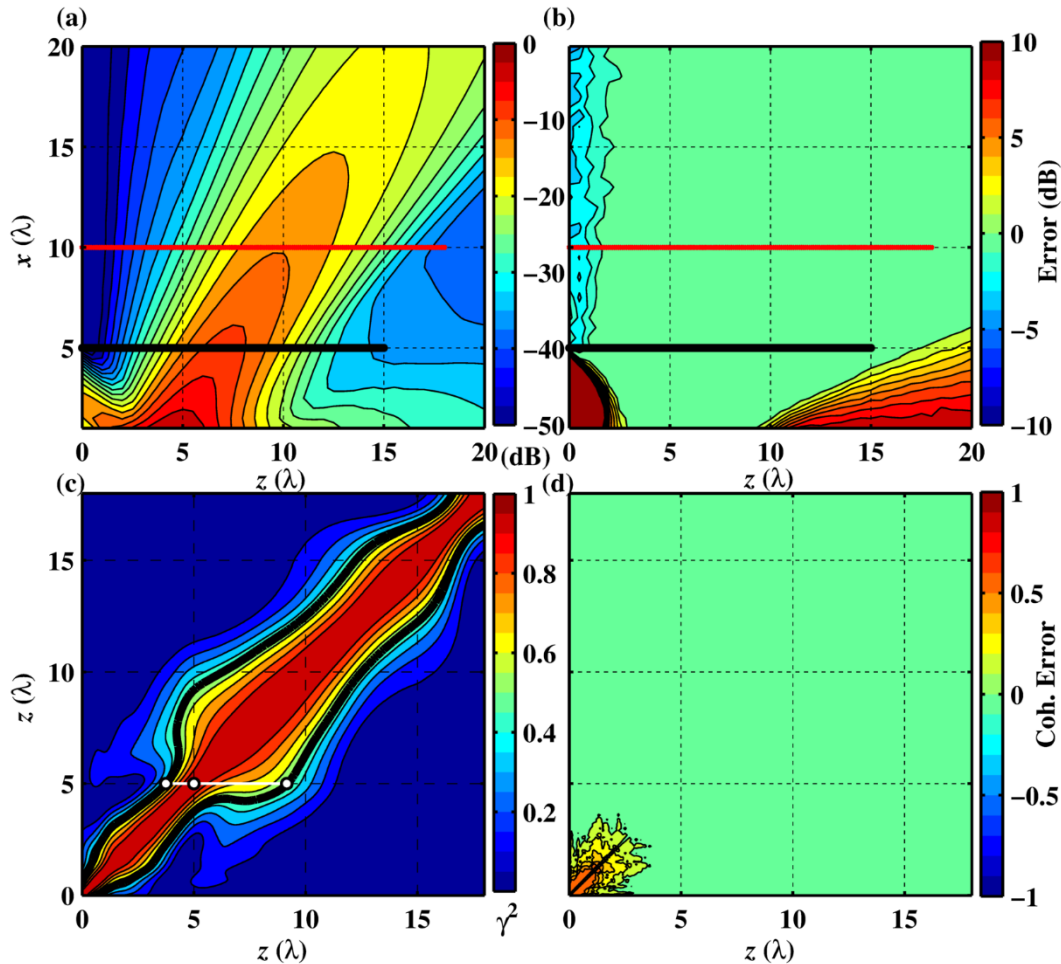


Figure 4. Multiple wavepacket beamforming. (a) The predicted acoustic field, generated by propagating the beamforming result of the multiple wavepacket example using the hybrid-beamforming method, is displayed, as well as (b) the level error between the field and the benchmark [in Figure 1(d)]. (c) The predicted coherence across the reference array [displayed as a red line in part (a)] from the propagated field is shown, and (d) the coherence error from the benchmark [Figure 2(b)] is given.

To more conveniently represent the spatial dependence of the coherence, coherence lengths, L_{γ^2} , are defined as the distance from a reference location over which coherence is significant ($\gamma^2 \geq 0.5$). This is illustrated by the white dots in Figure 4(c) for both upstream and downstream coherence lengths: at $z = 5\lambda$, $L_{\gamma^2} = 1.3\lambda$ in the upstream direction and $L_{\gamma^2} = 4.1\lambda$ downstream. Coherence length is an indicator of the spatiotemporal properties of the acoustic field, for a given frequency of interest, without the need to plot the entire coherence results across the array. The upstream and downstream coherence lengths from results in Figure 4(c) are provided in Figure 5, as well as the

benchmark coherence lengths [from Figure 2(b)] at the reference array. The predicted coherence lengths agree with the benchmark measurements to within 0.1λ except far upstream where the wavepacket source radiation was not significant. The asymmetry between the upstream and downstream coherence lengths can easily be seen, with the maximum coherence length occurring at $z = 9\lambda$ in the upstream direction and at $z = 5\lambda$ in the downstream direction. Using the source distribution generated by applying the hybrid-beamforming method to a linear array, both the acoustic field levels and its spatiotemporal properties have been accounted for.

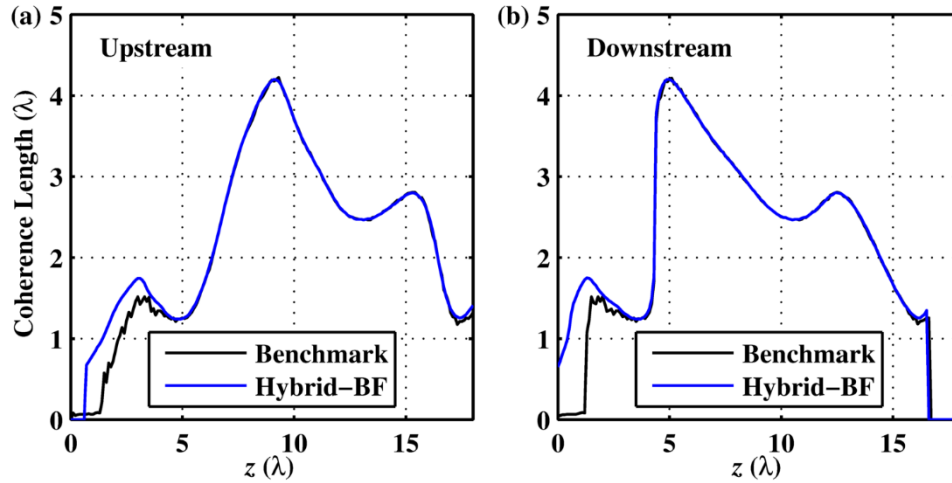


Figure 5. Coherence lengths of beamforming results. (a) Upstream and (b) downstream coherence lengths are calculated based on the coherence results shown in Figure 4(c). The benchmark coherence length measurements are plotted alongside.

III. Application to Full-Scale Measurement

In Section II the Hybrid Method was introduced and demonstrated to successfully reconstruct the overall source distribution, the field levels and coherence properties generated by a multiple-wavepacket source distribution. We now apply this method to measurements taken of supersonic jet noise from a full-scale installed military jet and compare the resultant acoustic field generated by a beamforming source solution to benchmark measurements.

A static single engine of an F-22A Raptor was measured at military engine condition (100% Engine Thrust Request) at Holloman AFB in 2009. Several nonsynchronous measurements were taken using a 90 microphone planar array [shown in Figure 6(a)], which moved to various locations marked by triangles in Figure 6(b). The result of these measurements was to create a two-dimensional measurement plane of nonsynchronous measurements that spanned 23.3 m by 2.0 m, with a two-dimensional measurement density of 15.24 cm. A fifty-element reference array was used to measure the field synchronously with every planar array measurement. Using the reference array, the nonsynchronous measurements were stitched together into partial fields that can then be utilized for inverse measurements (see Section II). This measurement aperture is expanded to provide increased resolution, by applying linear prediction. For further details on the experiment, see Ref. [18].

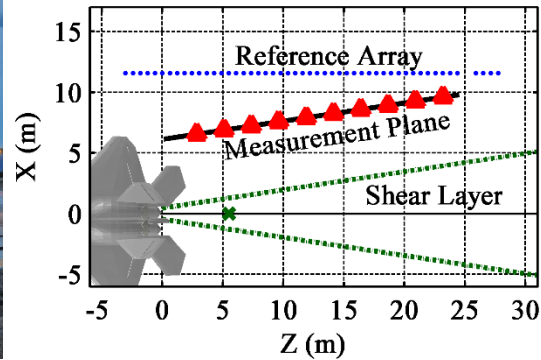


Figure 6. Measurement Setup. (a) A static firing of an F-22, with 90 microphone array mounted alongside. (b) The experimental setup is displayed with positions of the moveable 90 microphone array marked by red triangles, and a stationary 50 microphone reference array by blue dots.

The Hybrid method is applied to data on the measurement plane. The complex pressures from the measurement plane are used to form a cross-spectral matrix that is the input for the beamforming implementation, which assumes a one-dimensional source region along the jet centerline, as well as a virtual (image) source region mirrored about the ground. An example result from the application of hybrid-beamforming at a one-third-octave frequency of 250 Hz is shown in Figure 7(a). Here, the magnitude and the real part of the complex-beamforming solution is plotted on a linear scale. The result shows an equivalent acoustic source that is similar in structure to the mathematical wavepacket models previously described. While the overall phase of the source region is visible here, a single wavepacket representation cannot entirely simulate its characteristics (e.g., the coherence across the source). Instead, a system of wavepackets which combine to create this overall response would be a much more suitable representation.

The equivalent source distribution generated by the hybrid-beamforming results (i.e. “beamforming source”), is used to generate an acoustic field lying along the reference array, shown in Figure 7(b). Because this is propagated along the ground ($Y = 0$ m), reflection and interference patterns due to source reflections are not present, and the radiation amplitudes are approximately doubled. The acoustic radiation from the beamforming source shows a primary propagating radiation lobe at an angle about forty-five degrees relative to the jet centerline. A secondary lobe radiates in the downstream direction beginning at the centerline about $Z = 15$ m, although this lobe is not believed to be physical due to the inadequate coverage of the measurement array in this region.

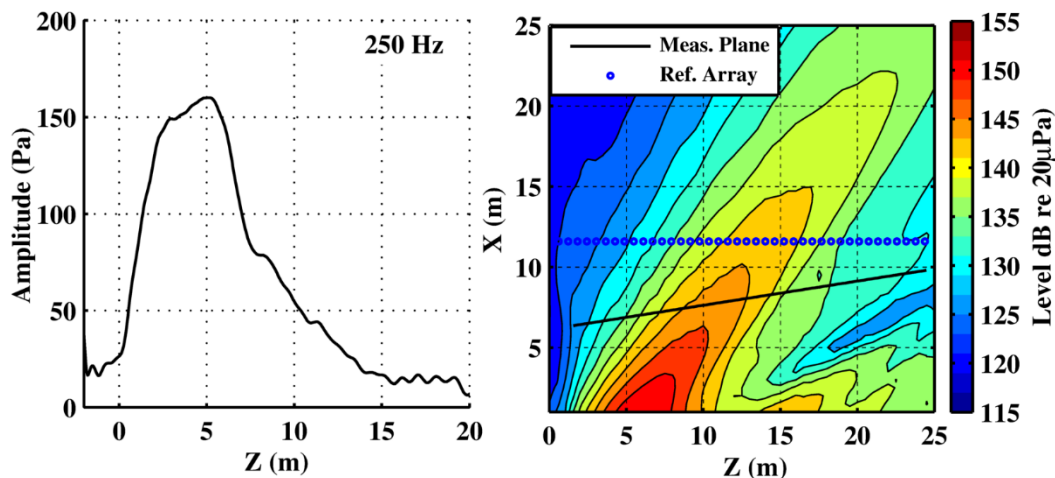


Figure 7. Beamforming results and propagated field. Hybrid beamforming is applied to F-22 measurements from the measurement plane at 250 Hz to generate (a) an equivalent acoustic source reconstruction magnitude and (b) the respective propagated field ($Y = 0$ m plane) from the beamforming source reconstruction.

The acoustic field generated from the beamforming source distribution can be compared to benchmark levels measured at the ground-based, reference array marked in Figure 6(b). The comparisons between the acoustic field

levels at the reference array to benchmark levels are shown in Figure 8 for octave-band center frequencies. Overall, the acoustic field measurements generated by the beamforming source show agreement with the measured levels to within about 2 dB for frequencies below 500 Hz. At 500 Hz, the top 10 dB of the benchmark levels match the generated field results within about 1dB. Measurements for larger Z values also show agreement with the generated field, although for $Z < 5$ m the generated field levels are significantly lower than benchmark levels. A likely explanation is that the number of significant partial fields generated at the measurement plane was inadequate to completely represent the source region at this frequency. This could also be an effect of the Tikhonov regularization in the hybrid-beamforming method, which attempts to suppress low-level features by treating them as noise. At 1000 Hz, only the top 3 dB of the benchmark levels are matched to the measurement with other levels 10-20 dB below the benchmark levels across the array, likely because of the same reasons described at 500 Hz.

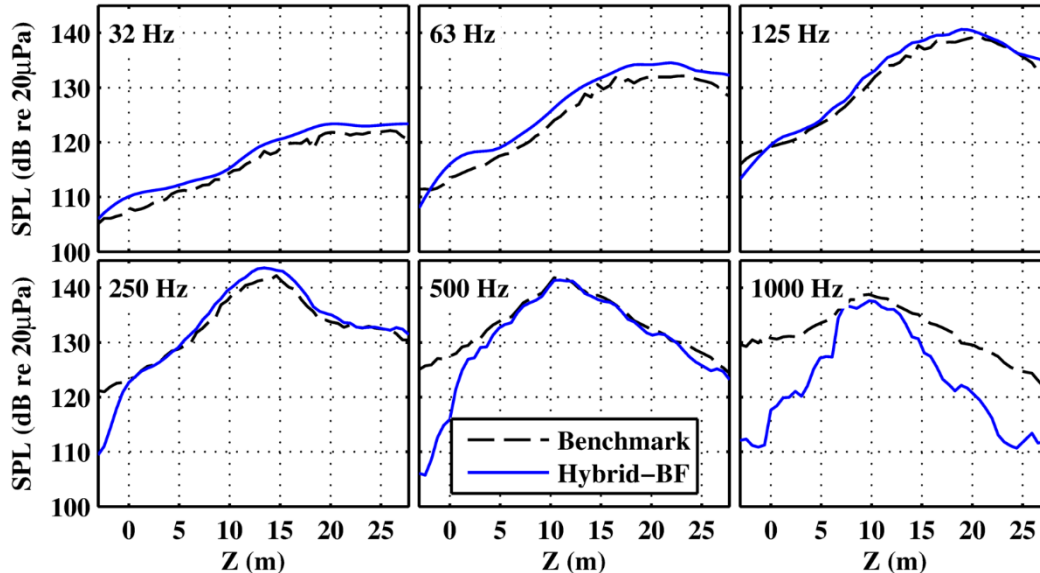


Figure 8. Propagated beamforming results. Benchmark levels at octave-band center frequencies of the F-22 measurements at the ground-based, reference array are compared to calculated levels obtained by propagating the beamforming reconstructions based on the measurement plane data.

The coherence lengths of the generated acoustic field are also compared to benchmark values at the reference array. The coherence lengths at the reference array locations are shown in Figure 9, with the benchmark coherence lengths presented as solid lines and the generated acoustic field values as dashed. For each frequency, both the upstream (displayed in blue with '+' markers) and the downstream (red with 'x' markers) coherence lengths are plotted together. At frequencies below 250 Hz, there is very good agreement in coherence lengths with benchmark measurements, within about 1 m at most array locations. At higher frequencies, the average coherence length decreases and results show agreement with the benchmark within 0.3 m, although in the downstream array region ($Z > 15$ m), the results begin to diverge somewhat. This is seen at 250 Hz and 500 Hz at about $20 \text{ m} < Z < 25 \text{ m}$, where the results are about 1.5 m higher than the benchmark values. This does not seem to be related to the error in the acoustic field levels with benchmark measurements as the levels for this frequency and location were within about 2 dB. At 1000 Hz, the average coherence length is below 1 m and approaches the resolution limit of the reference array spacing (0.61 m).

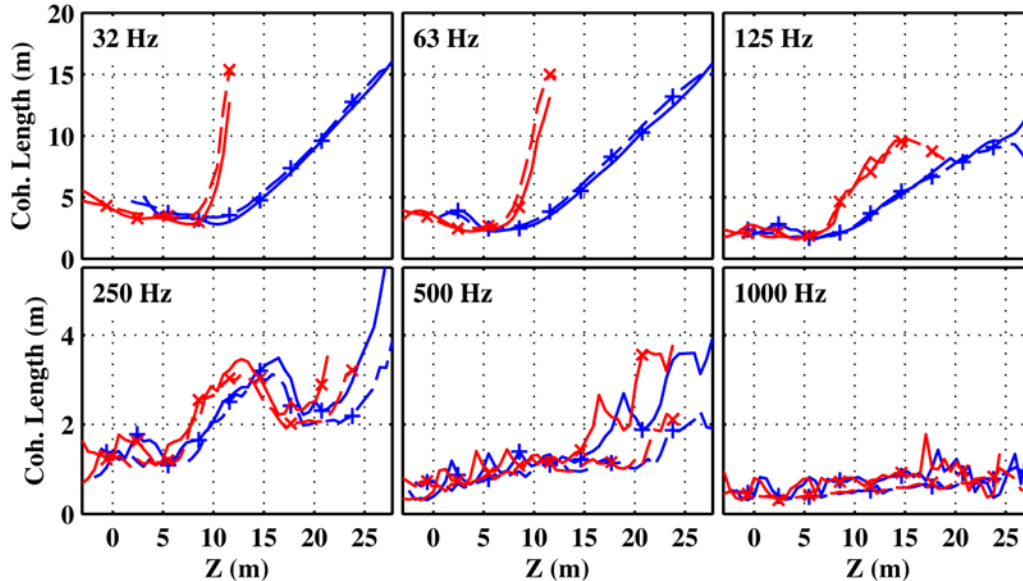


Figure 9. Coherence lengths from propagated beamforming results. Benchmark coherence lengths at octave-center frequencies measured at the ground-based array are given with the coherence lengths derived from complex pressures propagated from beamforming measurements originating at the measurement plane. Benchmark results are plotted as dashed lines and beamforming results as solid lines. Upstream coherence lengths are shown in blue with +’s and downstream coherence lengths are red with x’s.

The average error of the level measurements and coherence length measurements at the reference array are shown in Figure 10. The average error in level across the array is within about 2 dB for frequencies below 500 Hz and thereafter becomes significant, in part because of the microphone spacing. However, the average coherence length error is within 0.5 m at all frequencies shown, which is also limited by the microphone spacing. Overall, the predicted levels and coherence lengths derived from beamforming results an equivalent source region match the benchmark values with good agreement. This emphasizes that not only is it possible to effectively model jet noise source field levels, but the spatiotemporal characteristics of the field can also accurately be represented.

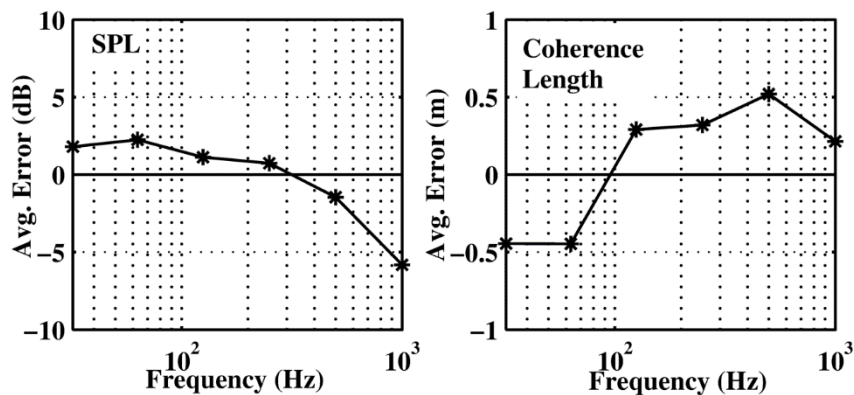


Figure 10. Error in average level and coherence length. The average errors in level and coherence length of the propagated beamforming results at the reference array relative to the benchmark levels and coherence lengths.

IV. Conclusion

Wavepacket models are valuable to simulate acoustic field radiation, in both the levels and coherence properties of the field. While nonunique, these characteristics contain an imprint of the physical source characteristics of the jet noise sources. In order to effectively simulate the field coherence properties, however, a multiple-wavepacket source representation is required. Examples of single and multiple-representation wavepackets have been presented, as well as their corresponding radiated fields and associated field coherence lengths. Beamforming methods that can operate on spatially extended, coherent sources are shown to effectively reconstruct the source magnitude and spatial

wavenumber component of a single radiating wavepacket distribution. In addition, the beamforming source reconstruction was used to predict an acoustic field similar to the benchmark field. This was also successfully done for a multiple-wavepacket source representation, where the levels and coherence lengths of the generated acoustic field agreed with benchmark measurements to within high precision. The Hybrid Method has also been applied to measurements taken of an installed F-22A engine operated at military engine power. Beamforming results of the equivalent source were used to generate an acoustic field, which was compared to separate measurements at a reference array. The predicted levels and coherence lengths at the reference array showed good agreement with benchmark results. Thus, beamforming methods which can predict not only levels of source radiation but also spatiotemporal characteristics at various field locations have been demonstrated as an effective means of generating a more accurate equivalent source representation.

Further studies should be designed to represent the beamforming source results as a convenient basis of wavepackets, similar to the multiple-wavepacket numerical sources used in the present paper. A preliminary attempt to decompose the beamforming source results using a singular-value decomposition—while successful at capturing the majority of the source levels in few eigenmodes—was unable to accurately reproduce the acoustic field levels and coherence lengths without requiring multiple tens of eigenmodes. Thus, a more effective means of reducing the beamforming results into a classification of wavepackets that can simply and effectively model the acoustic field is needed. Further improvements could also be made to the Hybrid method, including the choice of penalization parameter in the regularization technique, as well as the possible addition of deconvolution methods to help minimize array effects, which may show improvements over the current results. Improved prediction models of the acoustic radiation levels and coherence properties potentially allows for further physical understanding of jet noise and shows promise for noise environment modeling and noise reduction strategies.

Acknowledgments

This project was funded in part by the Office of Naval Research (ONR). Blaine M. Harker was funded in part by an appointment to the Student Research Participation Program at U.S. Air Force Research Laboratory, Human Effectiveness Directorate, Warfighter Interface Division, Battlespace Acoustics administered by the Oak Ridge Institute for Science and Education through an interagency agreement between the U.S. Department of Energy and USAFRL. The measurements were funded by the Air Force Research Laboratory through the SBIR program and supported through a Cooperative Research and Development Agreement (CRDA) between Blue Ridge Research and Consulting, Brigham Young University, and the Air Force.¹⁹ The authors would like to thank the F-22 program office for their review and clearance of the presented material. Distribution A: Approved for public release. 88ABW Cleared 12/4/2015; 88ABW-2015-5860.

References

- ¹Jordan, P. and Colonius, T., "Wave packets and turbulent jet noise," *Annual Review of Fluid Mechanics*, Vol. 45, 2013, pp. 173-195.
- ²Papamoschou, D., "Wavepacket modeling of the jet noise source," AIAA Paper 2011-2835, 2011.
- ³Morris, P., Dougherty, R., Nelson, C., Cain, A., and Brentner, K., "Wavepacket noise source model for microphone array data analysis of hot supersonic jets," *The Journal of the Acoustical Society of America*, Vol. 134, No. 5, 2013, pp. 4127-4127.
- ⁴Suzuki, T. and Colonius, T., "Instability waves in a subsonic round jet detected using a near-field phased microphone array," *Journal of Fluid Mechanics*, Vol. 565, No. 1, 2006, pp. 197-226.
- ⁵Du, Y. and Morris, P. J., "Numerical simulation of the effect of a low bypass cooling stream on supersonic jet noise," AIAA Paper 2014-1402, 2014.
- ⁶Brooks, T. F. and Humphreys Jr, W. M., "Extension of DAMAS phased array processing for spatial coherence determination (DAMAS-C)," AIAA Paper 2006-2654, 2006.
- ⁷Harker, B. M., Neilsen, T. B., Gee, K. L., James, M. M., and Wall, A. T., "Spatiotemporal Correlation Analysis of Jet Noise from a High-Performance Military Aircraft," AIAA Paper 2015-2376, 2015.
- ⁸Brooks, T. and Humphreys, W., "A Deconvolution Approach for the Mapping of Acoustic Sources (DAMAS) Determined from Phased Microphone Arrays," AIAA Paper 2004-2954, 2004.
- ⁹Sijtsma, P., "CLEAN based on spatial source coherence," *International Journal of Aeroacoustics*, Vol. 6, No. 4, 2007, pp. 357-374.
- ¹⁰Dougherty, R. P., "Improved generalized inverse beamforming for jet noise," *International Journal of Aeroacoustics*, Vol. 11, No. 3, 2012, pp. 259-290.
- ¹¹Padois, T., Berry, A., Gauthier, P.-A., and Joshi, N., "Beamforming matrix regularization and inverse problem for sound source localization : application to aero-engine noise," AIAA Paper 2013-2212, 2013.
- ¹²Dougherty, R. P., "Beamforming in acoustic testing," in *Aeroacoustic Measurements* (2002), pp. 62-97.
- ¹³Sarradj, E., "Three-Dimensional Acoustic Source Mapping with Different Beamforming Steering Vector Formulations," *Advances in Acoustics and Vibration*, Vol. 2012, No. 292695, 2012.

- ¹⁴Williams, E. G., "Regularization methods for near-field acoustical holography," *The Journal of the Acoustical Society of America*, Vol. 110, No. 4, 2001, pp. 1976-1988.
- ¹⁵Wall, A. T., Gee, K. L., Gardner, M. D., Neilsen, T. B., and James, M. M., "Near-field acoustical holography applied to high-performance jet aircraft noise," *Proceedings of Meetings on Acoustics*, Vol. 9, No. 1, 2011, pp. 040009.
- ¹⁶Neilsen, T., Gee, K., Harker, B., and James, M., "Level-educed Wavepacket Representation of Noise Radiation from the F-22A Raptor," AIAA Paper (submitted for publication), 2016.
- ¹⁷Reba, R., Narayanan, S., and Colonius, T., "Wave-packet models for large-scale mixing noise," *International Journal of Aeroacoustics*, Vol. 9, No. 4, 2010, pp. 533-558.
- ¹⁸Wall, A. T., Gee, K. L., James, M. M., Bradley, K. A., McInerny, S. A., and Neilsen, T. B., "Near-field noise measurements of a high-performance military jet aircraft," *Noise Control Engineering Journal*, Vol. 60, No. 4, 2012, pp. 421-434.
- ¹⁹SBIR DATA RIGHTS - (DFARS 252.227-7018 (JUNE 1995)); Contract Number: FA8650-08-C-6843; Contractor Name & Address: Blue Ridge Research and Consulting, LLC, 29 N Market St, Suite 700, Asheville NC; Expiration of SBIR Data Rights Period: March 17, 2016 (Subject to SBA SBIR Directive of September 24, 2002).